Biophysical Journal Volume 92 January 2007 115–125

Growth Dynamics of Domains in Ternary Fluid Vesicles

Miho Yanagisawa,* Masayuki Imai,* Tomomi Masui,* Shigeyuki Komura,† and Takao Ohta‡
*Department of Physics, Ochanomizu University, Bunkyo, Tokyo112-8610, Japan;†Department of Chemistry, Tokyo Metropolitan University, Tokyo 192-0397, Japan; and‡Yukawa Institute for Theoretical Physics, Kyoto University, Kyoto 606-8502, Japan

ABSTRACT We have studied the growth dynamics of domains on ternary fluid vesicles composed of saturated (dipalmitoylphosphatidylcholine), unsaturated (dioleoylphosphatidylcholine) phosphatidylcholine lipids, and cholesterol using a fluorescence microscopy. The domain coarsening processes are classified into two types: normal coarsening and trapped coarsening. For the normal coarsening, the domains having flat circular shape grow in a diffusion-and-coalescence manner and phenomenologically the mean size grows as a power law of $\sim t^{2/3}$. The observed growth law is not described by a two-dimensional diffusion-and-coalescence growth mechanism following the Saffman and Delbrück theory, which may originate from the two-body hydrodynamic interactions between domains. For trapped coarsening, on the other hand, the domain coarsening is suppressed at a certain domain size because the repulsive interdomain interactions obstruct the coalescence of domains. The two-color imaging of the trapped domains reveals that the repulsive interactions are induced by the budding of domains. The model free energy consisting of the bending energy of domains, the bending energy of matrix, the line energy of domain boundary, and the translation energy of domains can describe the observed trapped coarsening. The trapping of domains is caused by the coupling between the phase separation and the membrane elasticity under the incompressibility constraint.

INTRODUCTION

Biomembranes have characteristic lateral heterogeneities arising from the immiscibility of the lipid components such as sphingomyelin, unsaturated phospholipids, and cholesterol (Chol). In the so-called raft model, the heterogeneity coupled with the protein distribution plays important roles in the functionality of the biomembranes (1,2). Since the raft model has been suggested, extensive studies have been performed to reveal the composition, structure, dynamics, and physiological properties of the rafts. To realize the formation of rafts in artificial membranes, a ternary mixture consisting of saturated phospholipids, unsaturated phospholipids, and cholesterol has been studied (3–11). Such artificial membranes show a lateral phase separation below the miscibility transition temperature and form a liquid-ordered phase rich in saturated phospholipids and cholesterol, and a liquid-disordered phase rich in unsaturated phospholipids. Although the rafts in cell membranes and the domains in artificial membranes are not directly connected, the lateral phase separation in artificial membranes is a milestone to understand the raft structure.

From the membrane physics point of view, the domains in the model biomembrane vesicles show a quite unique nature. Veatch and Keller observed the liquid domain formation in giant vesicles consisting of DPPC (dipalmitoylphosphatidylcholine; saturated phospholipid), DOPC (dioleoylphosphatidylcholine; unsaturated phospholipid), and Chol using a fluorescence microscopy with Texas Red dipalmitoylphosphatidylethanolamine (TR-DPPE) dye (7–9). When the temperature is dropped from the homogeneous one-phase region to the two-phase region, the membrane is separated into a DPPC- and Chol-rich phase and a DOPC-rich phase (TR-DPPE is localized in the DOPC-rich region). Depending on the composition, such a phase separation exhibits two typical kinetic pathways, i.e., a nucleation-growth type and a spinodal decomposition type, although other more complicated patterns (e.g., viscous fingering pattern) have been reported (8). In the case of the nucleation-growth pathway, the circular domains grow by colliding and coalescing with other domains, whereas for the spinodal decomposition, a characteristic bicontinuous network pattern appears and then develops into circular domains. In both cases, the domains develop into a small number of large domains and eventually undergo a budding of domains (10,12). Similar domain coarsening processes have been observed in other ternary systems such as sphingomyelin/DOPC/Chol (3,4). The above mixed vesicles, however, sometimes show a unique long-lived hexagonal pattern with cap-shaped domains (10). Such an ordered domain structure suggests the existence of a long-ranged repulsive interdomain interaction, which may originate from the elastic nature of the membrane. Thus the domain coarsening in the fluid vesicles is strongly coupled with the membrane elasticity and the geometrical constraints.

The growth dynamics of domains in the fluid vesicles has been investigated theoretically by means of various simulation techniques such as the generalized time-dependent Ginzburg-Landau model (13,14), the dynamic triangulation Monte Carlo method (15), and the dissipative particle dynamics method (16–18). Using the time-dependent Ginzburg-Landau model, Taniguchi succeeded to reproduce cap-shaped domains on a vesicle (13). Due to the coupling between the vesicle shape and the phase separation, the vesicle exhibits a very slow coarsening process, where $D(t) \sim t^{a}$ ($D(t)$ is the average domain diameter and $a \sim 0.1$). The budding dynamics

Submitted May 5, 2006, and accepted for publication September 8, 2006.
Address reprint requests to Masayuki Imai, E-mail: imai@phys.ocha.ac.jp.

0006-3495/07/01/115/11 $2.00
doi: 10.1529/biophysj.106.087494

was investigated by Kumar et al. (15), using the triangulation Monte Carlo model, and they showed that, in the budding-coalescence regime, the number of buds decays as $N_{bud} \sim t^{-2/3}$. Recently Laradji and Kumar (16,17) investigated the growth dynamics of the domains using the dissipative particle dynamics and showed that the hydrodynamic interactions and the area/volume constraint strongly affect the domain growth. These approaches grasp the important features of the lateral phase separation in the fluid vesicles. However, it is still far from the quantitative understanding due to the lack of experimental studies on growth dynamics in the fluid vesicles.

In this article, we present a systematic experimental investigation on the growth dynamics of the domains in the fluid vesicles using fluorescence microscopy. After explaining our experimental method, we will classify the observed domain coarsening processes into two types, a normal nucleation growth mechanism and a trapped mechanism in the section ''Outline of domain coarsening in fluid vesicles''. The normal coarsening process will be characterized experimentally and then compared with the theoretical prediction for domain coarsening in the fluid membranes in the section ''Normal coarsening''. The dynamics of the trapped coarsening will be characterized in the section ''Trapped coarsening'', and the trapping mechanism will be discussed in terms of the coupling between the phase separation and the membrane elasticity under the area/volume constraint in the section ''Budding and area/volume ratio''. The criterion for the trapped coarsening will be examined using the free-energy expressions for a vesicle with budding domains in the section ''Free-energy analysis on trapped coarsening''. Finally we will summarize our study in the ''Conclusion''.

EXPERIMENTS AND ANALYSIS

Commercial reagents

DPPC (>99% purity) and DOPC (>99% purity) were obtained in a powder form from Avanti Polar Lipid (Alabaster, AL). Chol (>99% purity) was purchased from Sigma-Aldrich (St. Louis, Mo). All lipids were used without further purification. Mother solutions of lipids were stored in chloroform at −20°C until use. Texas Red dihexanoylphosphatidylethanolamine (TR-DHPE) and perylen were obtained from Molecular Probes (Eugene, OR), and used as a dye for contrast between liquid phases. TR-DHPE is localized in a liquid disordered (DOPC-rich) phase and shows a red color, whereas perylene partitions preferentially into a liquid ordered (DPPC- and Chol-rich) phase and shows a blue color (10).

Formation of giant vesicles

In this work, we fixed the ratio between the components comprising the vesicles at DPPC/DOPC/Chol = 4:4:2. Giant vesicles were prepared by the gentle hydration method (19,20). At first we dissolved the lipids, DPPC, DOPC, and Chol in 10 μl of chloroform (10 mM). To dye the DOPC rich phase, TR-DHPE was added at the ratio of 0.8:10 (dye/lipid). When we observe the both phases, we added TR-DHPE and perylene at the ratio of 0.8:10 and 1:500, respectively. The solvent was evaporated in a stream of nitrogen gas and the obtained lipid film was then kept under vacuum for 1 night to remove the remaining solvent completely. The dried lipid film was prewarmed at 60°C, and then we added 30 μl of pure water at 60°C. After 1 min of prehydration, the sample was hydrated with 970 μl of pure water at 60°C. During the hydration process, the lipid films spontaneously form giant vesicles with diameters of 10–150 μm.

Observation of giant vesicles using fluorescence microscope

The vesicle suspension was put on a glass plate with a silicon rubber spacer having the thickness of 0.5 mm, and then sealed with a cover glass immediately. This sample cell was set on the temperature control stage (Carl Zeiss, Oberkochen, Germany) with a precision of ±0.2°C. We observed the domain coarsening process using an inverted conformal microscope (Carl Zeiss, LSM 5) with either the laser-scanning mode or the Hg lamp mode. To avoid the domain formation before the observation, we paid special attention to keep the sample temperature above the melting temperature of DPPC (T_m, 41°C). For the observation of the vesicles, we decreased the temperature from the one-phase region (42–43°C) to the miscibility transition temperature with the rate of ~0.5°C/min or less. When the phase separation took place, we fixed the temperature immediately and the time evolution of domains was recorded with a charge-coupled device camera (Carl Zeiss, Axio Cam). For the observation of TR-DHPE dyeing systems, we used the laser scanning mode (λ = 543 nm) with 41002-B probe filter (CHROMA, Rockingham, VT; excitation/emission maxima ~575:640 nm). For the TR-DHPE and perylene dyeing systems, we used the Hg lamp mode with a modified XF-006 filter, which has the transmission of 80% in blue color region and 20% in red color region. To avoid photo-oxidation, we minimized the exposure to light.

Image analysis

The fluorescence microscope observation gives images of growing liquid-ordered domains (*black regions*) on a vesicle as shown in Fig. 1 *a*, where the arrows indicate the velocity of the domains. From the images, we made two histograms: distribution of the moving direction of domains and distribution of the interdomain distances. In the case of the image analysis, we focused on vesicles having a nearly spherical shape with a diameter of ~20 μm, because the field depth of the optical microscope was ~15 μm. To avoid image distortion effects owing to the curvature, we restricted

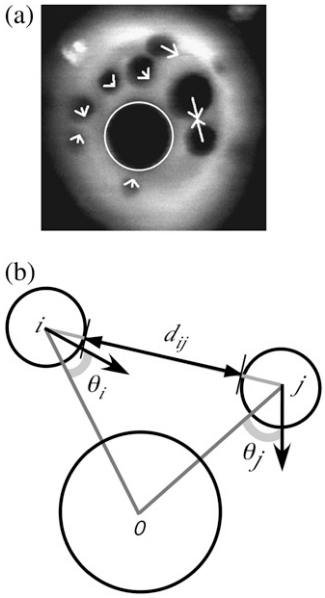

FIGURE 1 (*a*) Fluorescence microscope image of a vesicle with growing domains. Arrow indicates the velocity of the domain, and the largest domain is marked by a circle. Scale bar is 5 μm. (*b*) Parameters used to describe domain growth. The domain migration angle θ_i is that between the *i*th domain velocity direction (indicated by an *arrow*) and the line connecting the centers of the 0th largest domain and the *i*th domain. The interdomain distance d_{ij} is defined by the edge-to-edge distance between the centers of *i*th domain and *j*th domain.

the sampling area to the top hemisphere region with a radius of 5 μm, which gives maximum error of $\sim$10%. From the series of images, we estimated the distribution of the moving direction of domains with respect to the largest domain on the vesicle (marked by a *circle* in Fig. 1 *a*). In Fig. 1 *b*, we give the definition of the moving direction of a domain. The migration angle θ_i is that between the *i*th domain velocity direction (indicated by an *arrow*) and the line connecting the centers of the largest (0th) domain and the *i*th domain. For one vesicle, we extracted a total of 50 domains from the sequential images with a 1.5 s interval and obtained the distribution of the migration angle. The distributions from 10 vesicles were accumulated to obtain the distribution of the moving direction of domains. For the interdomain distance distribution analysis, to avoid the effect of domain size polydispersity, we measured the edge-to-edge distance d_{ij} between the centers of the *i*th domain and the *j*th domain as shown in Fig. 1 *b*. The histogram of the interdomain distances $h(d)$ was obtained from $\sim$100 pairs and the counts were divided by $2\pi d$.

Micropipette aspiration

To estimate the area/volume ratio of a vesicle, we adopted a micropipette aspiration technique (21). By micropipette aspiration, a flaccid spherical vesicle deforms to a tight vesicle. In this case, we are able to calculate the geometrical parameters. In this study, we used a micromanipulator (Narishige (Tokyo, Japan), MMO-202ND and MN-4) with a microinjector (Narishige, IM-9B) system. The floating target vesicle having a diameter of $\sim$100 μm is aspirated by the micropipette with an internal diameter of 20 μm. We increased the external suction pressure mildly until the vesicle deformed to a tight shape and then recorded its shape using the charge-coupled device camera.

RESULTS AND DISCUSSION

Outline of domain coarsening in fluid vesicles

First we show the short coarsening processes of the domains on the fluid giant vesicles having the composition of DPPC/DOPC/Chol = 4:4:2. When we decrease the temperature from the homogeneous one phase, the lateral phase separation between the liquid-ordered (L_o) and the liquid-disordered (L_d) phases takes place at 34°C (miscibility transition temperature, T_{mix}) with a nucleation-growth mechanism. In this study, we adopted the gentle hydration method to form the giant vesicles. The obtained vesicles have large polydispersities both in size and shape. This brings the diversity of the domain coarsening processes between the different vesicles (22). To improve statistical accuracy, we observed vesicles having nearly a spherical shape with a diameter of $\sim$20 μm. As a result of a large number of examinations, we found that the domain coarsening processes are classified into two types.

Fig. 2 shows the two types of the time evolutions of the domain growth at 30°C observed by the fluorescence microscope with TR-DHPE. For the both cases, we set $t = 0$ when the domain size reached to an optical resolution of the microscope ($\sim$0.8 μm). In Fig. 2 *a*, the circular domains (L_o phase) grew in a diffusion-and-coalescence manner while keeping the circular shape and reached to the size of $\sim$10 μm within several minutes. A similar coarsening

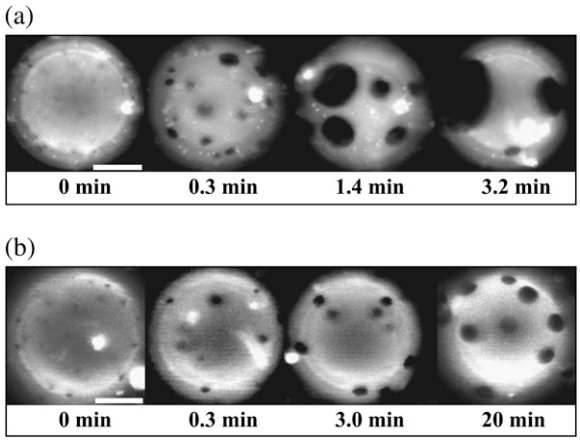

FIGURE 2 Time evolution of domain growth on a vesicle at 30°C observed by the fluorescence microscope; (*a*) normal coarsening and (*b*) trapped coarsening mechanisms. Scale bar is 5 μm.

process was reported in by Veatch and Keller (8). We call this coarsening process normal coarsening. In Fig. 2 *b*, on the other hand, the domain coarsening was trapped at a certain size for several 10 minutes. During the trapping period, the domains having almost the same domain size migrate on the vesicle without coalescence. We call this coarsening process as trapped coarsening. It should be noted that both coarsening processes are observed at the same time in the same microscope field.

To clarify the difference between normal coarsening and trapped coarsening, we plot the time evolution of the mean domain diameter $D(t)$ for the both cases in Fig. 3. For normal coarsening, phenomenologically the mean domain diameter $D(t)$ grew with a power law of $D(t) \sim t^{a}$ until the domains develop into a single large domain. The final monodomain state was stable for at least 1 day. For trapped coarsening, the mean domain size grew to $\sim$2 μm with the similar power law, and then the coarsening ceased for $\sim$100 min. After the trapping period, the domains restarted to grow toward a monodomain structure. We confirmed that the trapped coarsening can be reproduced by redoing the sample thermal history. When the temperature of the vesicle showing the trapped coarsening was increased above the transition temperature (corresponding to the homogeneous one-phase region) and then decreased below the phase separation temperature, we observed a similar trapped coarsening again. Analogous trapping phenomena (or slowing down of domain coarsening) were observed for vesicles having a hexagonal pattern (10) and vesicles having a large L_d phase fraction at low temperature (8). In our case, however, the domain (L_d phase) fraction was not so high, and each domain diffused freely on the vesicle surface as shown in Fig. 2 *b*. Thus we consider that trapped coarsening is a frequently observed coarsening process in fluid vesicles. In the following, we will discuss the mechanisms of the two different coarsening processes.

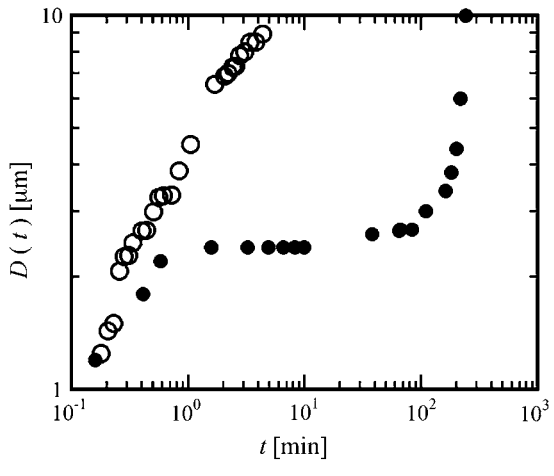

FIGURE 3 Time dependence of mean domain diameter $D(t)$ on a vesicle shown in Fig. 2, *a* and *b*. The open and closed circles denote normal and trapped coarsening, respectively.

Normal coarsening

To show the generality of the power law scaling of the normal coarsening, we plot in Fig. 4 *a* the time evolution of the domain diameter obtained from various normal coarsening vesicles with the composition of DPPC/DOPC/Chol = 4:4:2. Here we introduce the normalized diameter defined by $D_f^n(\tau_f) = D(\tau_f)/D_f$, where $D(\tau_f)$ is the mean diameter of the observed domains at time τ_f, and D_f is the diameter of the final monodomain. The normalized time is defined by $\tau_f = t/t_f$, where t_f is the time when the vesicle attains the monodomain structure. Roughly speaking, all the data collapse

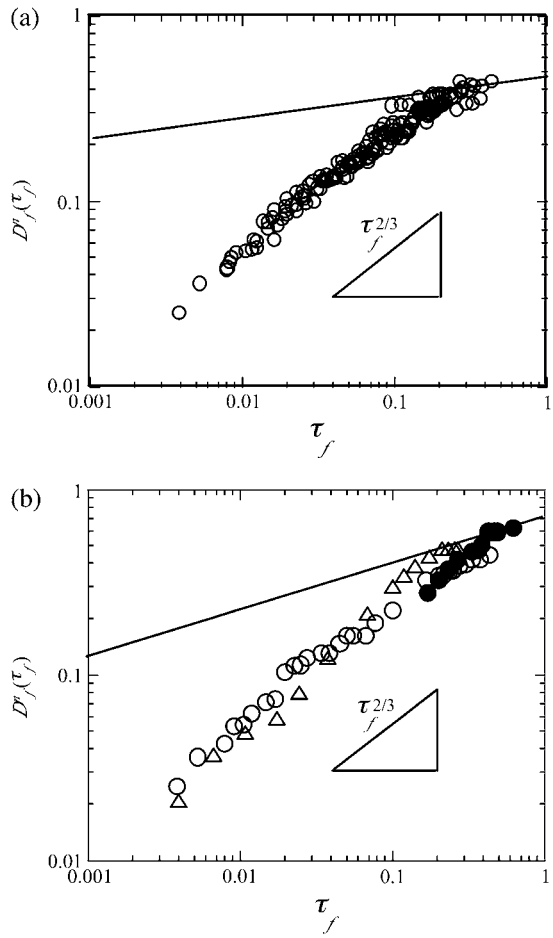

FIGURE 4 (*a*) Time dependence of normalized mean domain diameter of various vesicles with the composition of DPPC/DOPC/Chol = 4:4:2. The normalized diameter is expressed by $D_f^n(\tau_f) = D(\tau_f)/D_f$, where $D(\tau_f)$ is the mean diameter of the observed domains at time τ_f and D_f is the final monodomain diameter. The normalized time is expressed by $\tau_f = t/t_f$, where t_f is the time when the domains develop into the monodomain. A solid line and a triangle in the figure indicate the growth law of $D_f^n \sim \tau_f^{1/4}$ and the slope of $\tau_f^{2/3}$. (*b*) Time dependence of normalized mean domain diameter $D_f^n(\tau_f)$ in a vesicle with the various compositions. The open circles, triangles, and closed circles denote the composition of DPPC/DOPC/Chol = 4.5:4.5:1, 4:4:2, and 3:3:4, respectively. DPPC/DOPC/Chol = 3:3:4 sample showing spinodal decomposition mechanism, the data are taken from the late stage where domains have circular shape. A solid line and a triangle in the figure indicate the growth law of $D_f^n \sim \tau_f^{1/4}$ and the slope of $\tau_f^{2/3}$.

onto a single straight line, and the coarsening obeys the phenomenological power law growth $D(t)\sim t^{2/3}$. Furthermore, we examined the normal coarsening vesicles made with other compositions. Namely, we varied the fraction of cholesterol from 10% to 40% while keeping the ratio between DPPC and DOPC as 1:1. The obtained growth data are shown in Fig. 4 *b*. Here the vesicles containing Chol 35–40% showed the spinodal decomposition mechanism with bicontinuous textures. In these cases, we used the data from the late stage period in which the L_o phase forms circular domains. These results confirm the generality of the normal coarsening process characterized by the phenomenological growth law behavior $D(t) \sim t^{2/3}$.

To our knowledge, little is known about the growth law of the microdomains on the vesicles (16,17,23). Here we discuss the obtained growth law from a simple dynamical scaling point of view. The domain travels on the vesicle until it meets another domain. Once these two domains meet, they coalesce into one large domain. If we assume that each domain is regarded as a free Brownian particle and the average distance between neighboring domains is proportional to the average droplet diameter $D(t)$, the collision time Δt is expressed by

$$D(t)\sim(K\Delta t)^{1/2}, \tag{1}$$

where K is the diffusion constant of the domain. Since the droplet diameter increases by an amount roughly D for each coalescence, the increment of the diameter obeys the equation

$$\frac{\Delta D(t)}{\Delta t}\sim\frac{D(t)}{\Delta t}. \tag{2}$$

Then we obtained the expression

$$D(t)\sim(Kt)^{1/2}. \tag{3}$$

For the diffusion constant of a particle in a membrane, Saffman and Delbrück derived the following expression taking a two-dimensional hydrodynamic interaction coupled to an ambient fluid through the momentum dissipation mechanism (24,25):

$$K/k_BT=\frac{1}{4\pi\eta\delta}\left(\log\frac{\eta\delta}{\eta'(D/2)}-\gamma\right), \tag{4}$$

where k_B is the Boltzmann constant, T is the temperature, η and η' are the viscosities of the membrane and the exterior liquid, respectively, δ is the thickness of membrane, and γ is Euler's constant (= 0.5772). Here we should note that the above expression is an asymptotic form when the rate of momentum dissipation to the surrounding medium is small, i.e., $\eta' D/\eta\delta \ll 1$. By putting typical values for the membrane system, $\eta = 1$ poise, $\eta' = 0.01$ poise, $\delta = 5$ nm and $D = 5\mu$m, we obtain $\eta' D/\eta\delta = 10$, which does not satisfy the necessary condition for the Saffman and Delbrück equation (Eq. 4). This is due to the fact that the dissipation rate of a large domain is not small compared with that of a small particle like a protein or lipid molecule with the size of several nanometers. When the momentum dissipates rapidly from the membrane to the surrounding medium, i.e., $\eta' D/\eta\delta \gg 1$, the diffusion constant was derived by Komura and Seki (25) and is given by

$$K/k_BT\approx\frac{1}{\pi\eta\delta}\left(\frac{\eta\delta}{\eta' D}\right)^2. \tag{5}$$

In this case, we obtain the growth law of $D \sim t^{1/4}$. This growth law is shown in Fig. 4, *a* and *b*, by a solid line. Unfortunately, this scaling law does not describe our experimental data. One candidate to explain this disagreement is that the assumption of the free Brownian particle (Eq. 1) does not hold for the migrating domains on a vesicle.

We consider that the key concept to understand our experimental result is the hydrodynamic interactions between the domains. In Fig. 5 *a*, we show the movement of the center of gravity of each domain by an arrow during the time interval of $\Delta t = 1.5$ s. Instead of moving randomly, each domain seems to be attracted toward the largest target domain following the flow around the domain. We estimated the distribution of the moving direction of domains with respect to the largest domain in the vesicle (marked by a *circle*). Details of the image analysis were described above. The migration angle θ_i is that between the domain velocity direction (indicated by an *arrow*) and the line connecting the centers of the largest domain and the *i*th domain as shown in

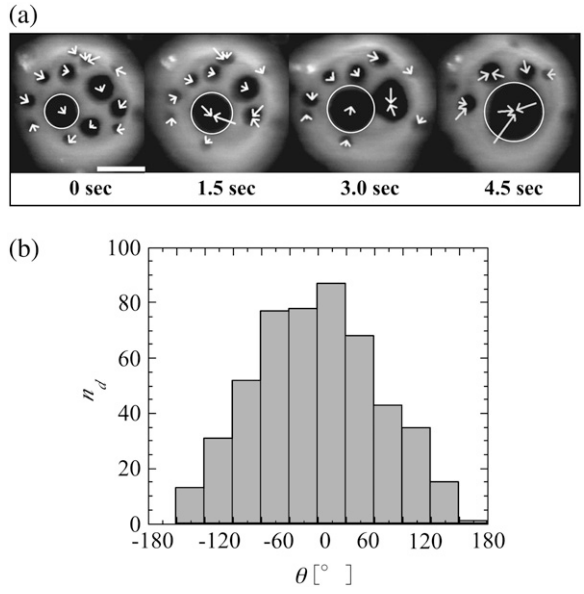

FIGURE 5 (*a*) Time sequence of migrating domains on a vesicle with normal coarsening. Arrow indicates the movement of the center of gravity of the domain during the time interval $\Delta t = 1.5$ s. The largest domain is marked by a circle and the scale bar denotes 5 μm. (*b*) Distribution of domain migration angle θ defined in Fig. 1 *b*. The vertical axis indicates the number of domains, n_d.

Fig. 1 *b*. In Fig. 5 *b*, we plotted the distribution of θ for the normal coarsening domains in the early stage, where n_d is the number of domains. When the domains behave as free Brownian particles, the distribution of θ should be uniform. However, the experimentally obtained distribution has a Gaussian profile with a mean value of $\sim 0°$ and a variation of $\sim 76°$, indicating that the domains tend to move toward the target domain. We consider that this motion is due to the two-body hydrodynamic interaction, which results in the deviation from the theoretical prediction described above. The coupling between the phase separation and the diffusion in membranes with hydrodynamic interaction may play an important role to understand the observed normal coarsening behavior (26–28) and will be addressed in our forthcoming article.

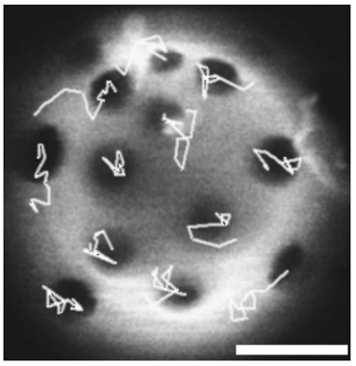

FIGURE 7 Loci of several trapped domains during 60 s projected on a vesicle image.

Trapped coarsening

In contrast to normal coarsening, trapped coarsening is characterized by a significant slowing down of the domain growth as shown in Fig. 3. In Fig. 6, we plot the time dependence of the domain diameter obtained from various vesicles with the composition of DPPC/DOPC/Chol = 4:4:2. The mean size of the trapped domains and the onset times of the trapping differ among the vesicles. Hence we introduce the normalized diameter defined by $D_i^n(\tau_i) = D(\tau_i)/D_i$, where D_i is the mean domain diameter at the onset of the trapping. Similarly, the normalized time is defined by $\tau_i = t/t_i$, where t_i is the onset time of the trapping. To elucidate the mechanism of the trapped coarsening, the traces of several trapped domains during 60 s are shown in Fig. 7. The traces show that each domain is localized in a certain cage, and the domains tend to repel each other when they approach. Such a repulsive interaction can be effectively extracted from the radial distribution function of the domains. Unfortunately, owing to the limitation of the microscope visibility and the finite number of the domains on the vesicles, we cannot obtain the reliable radial distribution function from the microscope images. Instead, we measured the distance distribution $h(d)$, which represents the number of domains n_d with the interdomain distance d (to avoid the effect of domain size polydispersity, we measured the edge-to-edge distances between the centers of the domains). Details of the image analysis were described above. The normalized distance distribution histogram has a peak at $\sim 1.6\ \mu$m as shown in Fig. 8. This indicates the existence of a repulsive interdomain interaction at short length scale. If we assume that the trapped domains are in a temporal equilibrium state and the area fraction of domains is low, the

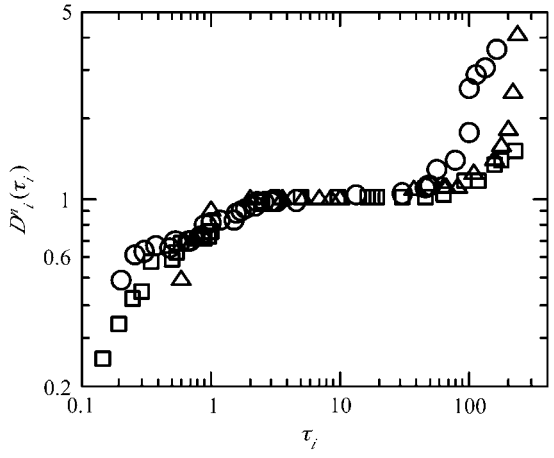

FIGURE 6 Time dependence of normalized mean domain diameter obtained from various trap coarsening vesicles with composition of DPPC/DOPC/Chol = 4:4:2. Normalized diameter is expressed by $D_i^n(\tau_i) = D(\tau_i)/D_i$. D_i is the mean domain diameter at the onset time of the trapping and τ_i is the normalized time expressed by $\tau_i = t/t_i$ where t_i is the onset time of the trapping.

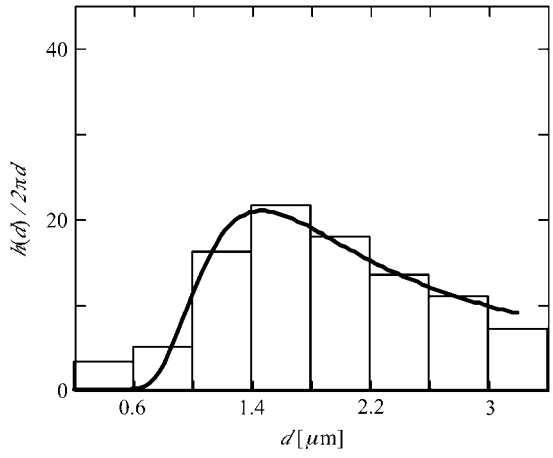

FIGURE 8 Histogram of the interdomain distance $h(d)$ for trapped domains. To avoid the effect of domain size polydispersity, we measured edge-to-edge distances between centers of two circular domains (see Fig. 1 *b*). A solid curve indicates $h(d)/2\pi d \sim \exp(-u(d)/k_BT)$ with $u(d) = u_r(\frac{\bar{D}}{d})^2 - u_a(\frac{\bar{D}}{d})$. The values used in this fitting are $\bar{D}$=1.8 μm, $u_r \sim 12\ k_BT$, and $u_a \sim 11.9\ k_BT$.

normalized histogram is approximately expressed by the interaction potential $u(d)$ through the Boltzmann distribution

$$h(d)/2\pi d \sim \exp(-u(d)/k_{\mathrm{B}}T). \quad (6)$$

The histogram can be reproduced by assuming a phenomenological interdomain potential such that

$$u(d) = u_{\mathrm{r}}\left(\frac{\bar{D}}{d}\right)^{2} - u_{\mathrm{a}}\left(\frac{\bar{D}}{d}\right), \quad (7)$$

where $\bar{D}$ is the mean diameter of the domains of the ensemble. The first and the second terms represent the repulsive and the attractive interdomain potentials, respectively. As shown by the solid curve in Fig. 8, the observed histogram is well described by Eq. 7 with the parameter values of $u_{\mathrm{r}} \sim 12\ k_{\mathrm{B}}T$ and $u_{\mathrm{a}} \sim 11.9\ k_{\mathrm{B}}T$. The obtained repulsive potential is responsible to the loci of the trapped domains in Fig. 7. Moreover, the value of $u_{\mathrm{r}} \sim 12\ k_{\mathrm{B}}T$ is comparable to the bending modulus of the DOPC matrix membrane, which is $\sim 20\ k_{\mathrm{B}}T$. The phenomenological attractive interaction in the large interdomain distance may arise from two contributions: one is the limitation of the Boltzmann distribution approximation (low area fraction approximation) and the other is that the domains tend to move toward the target domain as shown in Fig. 5 *b*.

To elucidate the difference between normal and the trapped coarsening, we dyed not only the matrix (L_d phase) but also the domains (L_o phase). TR-DHPE localized in the L_d phase emits red fluorescence, whereas the perylene prefers the L_o phase and emits blue fluorescence. The two regions dyed with different colors can be observed simultaneously using a modified filter that has high transmission for blue color and low transmission for red color. Fig. 9, *a* and *b*, are the time evolution of the two color cross-section images for the normal coarsening and the trapped coarsening domains, respectively. For normal coarsening, the domains do not bud and have the average curvature that is equal to that of the surrounding matrix. In this case, the coarsening proceeds straightway and the vesicle keeps its spherical shape during coarsening. On the other hand, in the case of trapped coarsening, the domains have the same curvatures as the surrounding matrix in the initial coarsening stage, although the cross section of the vesicle is flaccid. With the elapse of time, the domain grows to a certain size and then buds to a cap-like shape. This observation indicates that the line energy of domains starts to play a dominant role on the domain morphology (12). It is important to note that the onset time of the domain budding coincides with that of the domain trapping.

The simplest model to explain the observed repulsive interaction is the bending penalty of the matrix membrane between the two approaching cap-shaped domains. When the domains slightly bud toward the outside of the vesicle (cap-shaped domains), the matrix membrane surrounding the cap-shaped domain is deformed to skirt-like shape, accordingly. A cross-section image of the vesicle with the trapped domains (Fig. 9 *c*) supports the fact that the geometry of the surrounding matrix is a skirt-like shape. When the two cap-shaped domains approach, the curvature of the skirt-like region becomes large ($\sim 1/d$), which results in a repulsive potential between the two domains ($\sim 1/d^2$). In contrast, if the domains are not bud and have the same curvature with the matrix membrane, the approaching two domains are not blocked by the matrix membrane, which gives rise to the coalescence of the domains. Thus we conclude that the bending of the matrix membrane between the two approaching cap-shaped domains induces the repulsive interaction, which in turn results in the trapped coarsening.

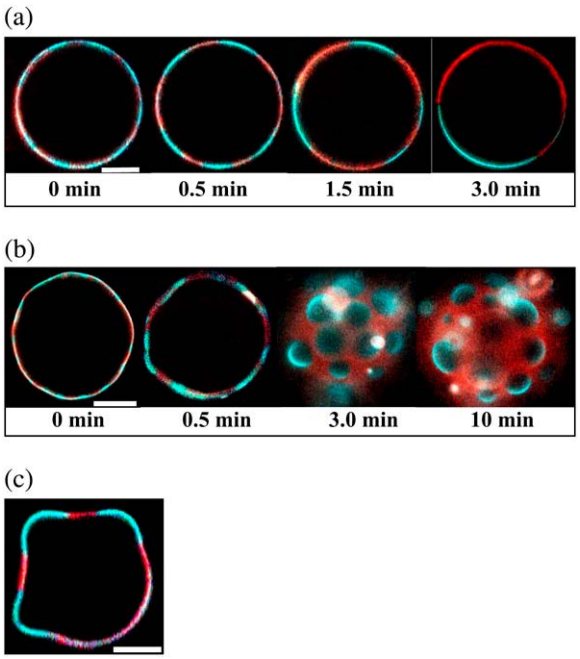

FIGURE 9 Time evolution of two color (TR-DHPE and perylene) cross-section images for normal coarsening vesicle (*a*) and trapped coarsening vesicle (*b*). To show the budding domains clearly, the focusing points are at the top of vesicles for 3.0 and 10 min images in *b*. (*c*) Two color cross-section images for budding domains in the trapped coarsening vesicle. Scale bar in figures is 50 μm.

Budding and area/volume ratio

According to the theory of budding (12), the budding is governed by the balance between the membrane bending energy and the line energy at the domain boundary. The important aspect of the trapped coarsening is the coupling between the phase separation and the membrane elasticity. When the budding occurs, however, there is another important constraint, i.e., the incompressibility of the membrane. Because of the equality of the osmotic pressure between inside and outside of the vesicle membranes, we consider that the area/volume ratio of the vesicle is constant during the coarsening process. This assumption was confirmed

experimentally by a micropipette aspiration technique as shown later. Here we discuss the geometrical constraints for the budding based on the following assumptions: 1), all domains are cap-like shape of the same size with a curvature of $1/a$; 2), the matrix is represented as a perforated spherical film with a curvature of $1/b$ (there is a discontinuity of the curvature at the boundary of the domain); and 3), the total surface area and the total volume of a vesicle are conserved. The geometrical parameters used in the following calculation are defined in Fig. 10.

We consider a vesicle with n_d cup-shaped domains. The total surface area of the vesicle S is a sum of those of the domains S_d and the matrix S_m,

$$S = S_d(n_d) + S_m(n_d) = 4\pi R_S^2, \tag{8}$$

where we introduce a surface area-based radius R_S. The total domain area S_d is given by

$$S_d(n_d) = n_d\left\{4\pi a^2 \sin^2\left(\frac{\alpha}{2}\right)\right\} = \pi L^2, \tag{9}$$

where L is the radius of a flat circular disk with the area S_d and the angle α is defined in Fig. 10. The total area of the matrix S_m is given by

$$S_m(n_d) = 4\pi b^2 - n_d\left\{4\pi b^2 \sin^2\left(\frac{\beta}{2}\right)\right\}, \tag{10}$$

where the angle β is defined in Fig. 10. On the other hand, the total volume of a vesicle with n_d cap-shaped domains V is expressed as a sum of the domain part V_d and the matrix part V_m, thus

$$V = V_d(n_d) + V_m(n_d) = \frac{4}{3}\pi R_V^3 \tag{11}$$

$$V_d(n_d) = n_d\left\{\frac{4}{3}\pi a^3 \sin^2\left(\frac{\alpha}{2}\right) - \frac{1}{3}\pi(a\sin\alpha)^2(a\cos\alpha)\right\} \tag{12}$$

$$V_m(n_d) = \frac{4}{3}\pi b^3 - n_d\left\{\frac{4}{3}\pi b^3 \sin^2\left(\frac{\beta}{2}\right) - \frac{1}{3}\pi(b\sin\beta)^2(b\cos\beta)\right\}, \tag{13}$$

where R_V is the volume-based radius. The area/volume ratio plays an important role in the budding behavior of the vesicle. In this study, we introduce a parameter ''dimensionless excess radius ξ'' to measure the area/volume ratio, which is defined by

$$\xi \equiv \frac{R_S - R_V}{R_V}. \tag{14}$$

In case of $\xi = 0$, the vesicle takes a perfect spherical shape and there is no room for the budding, even if the gain in the line energy overcomes the cost in the membrane bending energy. Increase of ξ means increase of the area/volume ratio, or the excess area, which allows the domains to bud.

The dimensionless excess radius ξ can be estimated using a micropipette aspiration technique. By the aspiration, the excess area of the vesicle forms a subsystem in the micropipette as shown in Fig. 11. The deformed vesicle consists of a spherical cap part with the radius R_1 (subsystem 1), and a cylindrical part (length l) with a hemispherical cap with the radius R_2 (subsystem 2). Assuming that the total volume and the total surface area are conserved during the aspiration, we can calculate the total volume and the total surface area from the following geometrical relations:

$$S = 4\pi\left(R_1^2\left(1 - \sin^2\left(\frac{\varphi}{2}\right)\right) + \frac{R_2^2}{2}\right) + 2\pi R_2 l = 4\pi R_S^2. \tag{15}$$

$$V = \frac{4}{3}\pi\left(R_1^3\left(1 - \sin^2\left(\frac{\varphi}{2}\right)\right) + \frac{R_2^3}{2}\right) + \frac{1}{3}\pi R_2^2 R_1 \cos\varphi + \pi R_2^2 l = \frac{4}{3}\pi R_V^3. \tag{16}$$

The excess radius ξ can be calculated from the experimentally obtained R_1, R_2, l, and ϕ. First, to examine the conservation law of the total area and the total volume of a vesicle, we measured them before and after the phase separation and confirmed the conservation law. Then we obtained the distribution of ξ for the vesicles showing the normal coarsening and the trapped coarsening as shown in

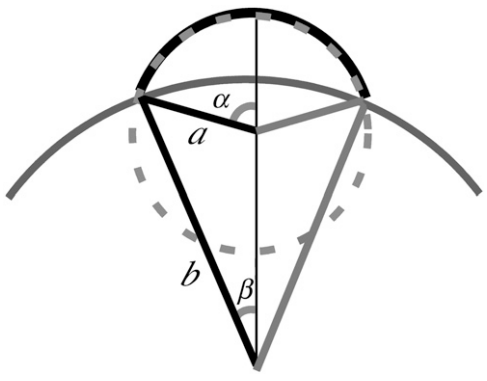

FIGURE 10 Geometrical model describing a cap-shaped domain on a vesicle. The domain has a curvature of $1/a$ and the matrix has a curvature of $1/b$.

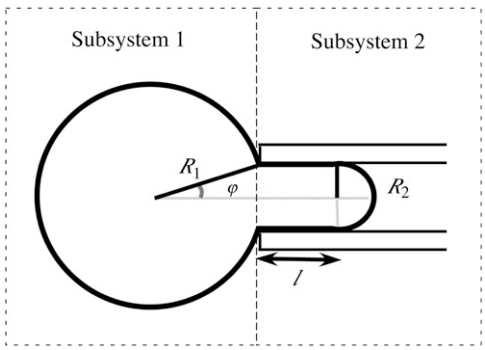

FIGURE 11 Schematic representation of aspirated vesicle with micropipette. By the aspiration, the vesicle is divided into two subsystems. Subsystem 1 has spherical cap geometry with radius R_1 and subsystem 2 is a cylinder with a hemispherical end cap, characterized by radius R_2 and length l.

Fig. 12, where n_v is the number of vesicles. For the vesicles with the normal coarsening domains (*white bar*), the values of ξ are distributed in the range of 0–0.01. The small ξ for the normal coarsening indicates that the vesicle has a nearly spherical shape. On the other hand, for the trapped coarsening (*gray bar*), the values of ξ are distributed in the range of 0.01–0.06. Thus the trapped coarsening vesicle has a flaccid spherical shape. These results are consistent with the fluorescence microscope observation shown in Fig. 9, *a* and *b*. These results confirm that the condition whether the vesicle shows the trapped coarsening or the normal coarsening is determined by the value of ξ and the experimentally obtained threshold is $\xi^* \sim 0.01$. It is interesting to note that the excess area of the spherical subsystem 1 of the vesicle is extremely decreased by the aspiration. Then the trapped domains start to coalesce and finally form a large monodomain at the neck of the aspirated vesicle.

Free-energy analysis on trapped coarsening

Here we perform a free-energy analysis of the phase-separating vesicle with the excess area. The free energy per vesicle having n_d cap-shaped domains consists of i), the bending energy of the domains E_d^{cap}; ii), the bending energy of the matrix E_m^{cap}; iii), the line energy at the domain boundaries E_l^{cap}; and iv), the energy associated with the translational entropy of the domains E_{tr}^{cap}. Under the geometrical constraints expressed by Eqs. 8–13, each contribution is given by

$$E_d^{cap} = n_d\left\{\frac{1}{2}\kappa_d\left(\frac{2}{a}\right)^2 S_d(n)\right\} = \frac{2\kappa_d\pi L^2}{a^2} \tag{17}$$

$$E_m^{cap} = \frac{1}{2}\kappa_m\left(\frac{2}{b}\right)^2 S_m(n_d) = 8\pi\kappa_m\left\{1 - n_d\sin^2\left(\frac{\beta}{2}\right)\right\} \tag{18}$$

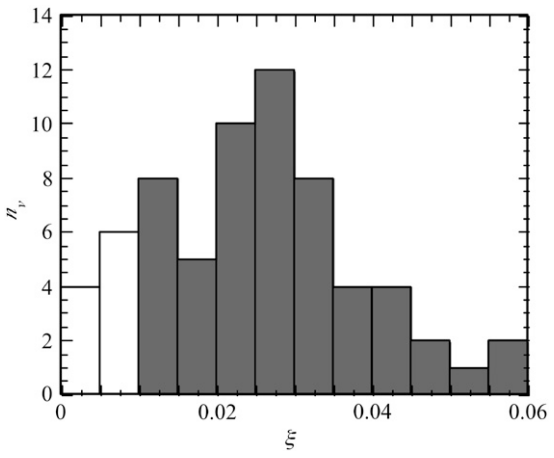

FIGURE 12 Distribution of excess area ξ for normal coarsening vesicles (*white bar*) and trap coarsening vesicles (*gray bar*) obtained by micropipette aspiration technique. The vertical axis denotes the number of vesicles n_v.

$$E_l^{cap} = 2\pi\sigma\frac{L}{\sqrt{n_d}}\sqrt{1 - \left(\frac{L}{2a\sqrt{n_d}}\right)^2} \tag{19}$$

$$E_{tr}^{cap} = n_d k_B T\log\phi, \tag{20}$$

where κ_d and κ_m are the bending moduli of the domain and the matrix, respectively, σ is the line tension at the domain boundary, and ϕ is the area fraction of the domains. Here the spontaneous curvature of the membrane is assumed to be zero. The excess radius ξ is taken into account by the relation

$$\pi L^2 = \phi S = \phi 4\pi R_s^2 = \phi 4\pi[R_V(1+\xi)]^2. \tag{21}$$

Then the total free energy of a vesicle with n_d cap-shaped domains is expressed by

$$E_{total}^{cap} = E_d^{cap} + E_m^{cap} + E_l^{cap} + E_{tr}^{cap}. \tag{22}$$

Here we assume that all the domains inevitably bud in the presence of the excess area as shown in Fig. 10.

To obtain the condition whether the domains bud or not, we have to estimate the free energy of a vesicle having the same ξ but without any budding domains. In this case, the mean curvature of the domain is equal to that of the matrix, i.e., hereafter we call it a flat (nonbudding) domain. When we calculate the total free energy of such a vesicle, we approximated the vesicle as a sphere with radius R_s, i.e., $a = b = R_S = R_V(1+\xi)$. The free energy per vesicle with n_d flat domains is expressed by

$$E_{total}^{flat} = E_d^{flat} + E_m^{flat} + E_l^{flat} + E_{tr}^{flat} \tag{23}$$

$$E_d^{flat} = n_d\left\{\frac{1}{2}\kappa_d\left(\frac{2}{R_V^2}\right)^2\left(\frac{4\pi R_V^2}{n_d}\right)\phi\right\} = 8\pi\phi\kappa_d \tag{24}$$

$$E_m^{flat} = \frac{1}{2}\kappa_d\left(\frac{2}{R_V^2}\right)^2 4\pi R_V^2(1-\phi) = 8\pi\kappa_m(1-\phi) \tag{25}$$

$$E_l^{flat} = 4\pi\sigma R_V(1+\xi)\sqrt{\frac{\phi}{n_d}\left(1 - \frac{\phi}{n_d}\right)} \tag{26}$$

$$E_{tr}^{flat} = n_d k_B T\log\phi. \tag{27}$$

In the free-energy analysis, the lengths a and L are scaled by the radius R_V and we introduce the dimensionless total free energy $\bar{E}_{total}^{i} = E_{total}^{i}/2\pi\kappa_d$ (i = cap or flat).

The obtained free energies of a vesicle with cap-shaped domains $\bar{E}_{total}^{cap}$ and with flat domains $\bar{E}_{total}^{flat}$ are plotted as a function of the number of domains n_d on a vesicle in Fig. 13, where we used the values of $\phi = 0.4$, $\kappa_d/\kappa_m = 1.25$, and $\kappa_d/\sigma = 0.2$ μm (10,29). For the vesicle with a large excess radius ($\xi = 0.116$; *black lines*), the free energies for $\bar{E}_{total}^{cap}$ (*solid line*) and $\bar{E}_{total}^{flat}$ (*dashed line*) decrease with decreasing n_d. The flat domains have lower energy for $n_d > 110$, whereas the cap-shaped domains are more favorable for $n_d < 110$. Thus the budding transition is expected to take place at $n_d^* \sim 110$. This means that when the domain grows to the threshold

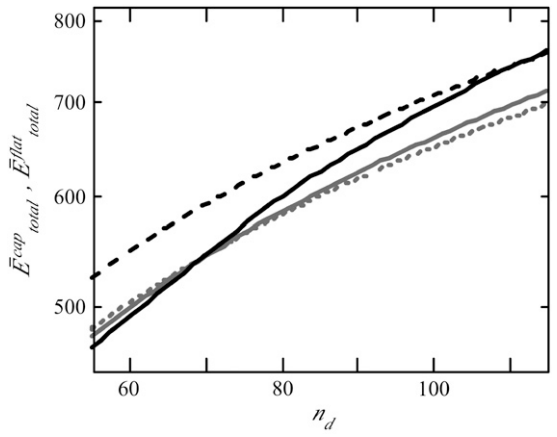

FIGURE 13 Free-energy curves of a vesicle with cap-shaped domains $\bar{E}^{cap}_{total}$ (*solid lines*) and with flat domains $\bar{E}^{flat}_{total}$ (*dashed lines*) as a function of number of domains n_d. Black and gray lines correspond to a vesicle with large excess area ($\xi = 0.116$) and small excess area ($\xi = 0.025$), respectively.

size determined by $(\pi L^2/n_d^*)^{1/2}$, the domain starts to bud. Recalling that the onset time of the budding transition coincides with that of the trapped coarsening, n_d^* corresponds to the number of the trapped domains on a vesicle and $(\pi L^2/n_d^*)^{1/2}$ is the mean size of the trapped domains.

This threshold strongly depends on the value of ξ. In the case of the smaller excess radius ($\xi = 0.025$; *gray lines* in Fig. 13), the budding transition takes place at $n_d^* \sim 70$. Further decrease of ξ results in $n_d^* = 1$, where budding transition does not take place on the vesicle, and hence the normal coarsening occurs. This critical excess radius ξ^* determines whether the vesicle exhibits trapped coarsening or normal coarsening. To estimate the value of ξ^*, we measured the number of domains in the trapped state, n_d, as a function of ξ as shown by open circles in Fig. 14. The normal coarsening vesicles (corresponding to $n_d = 1$) have very small values of

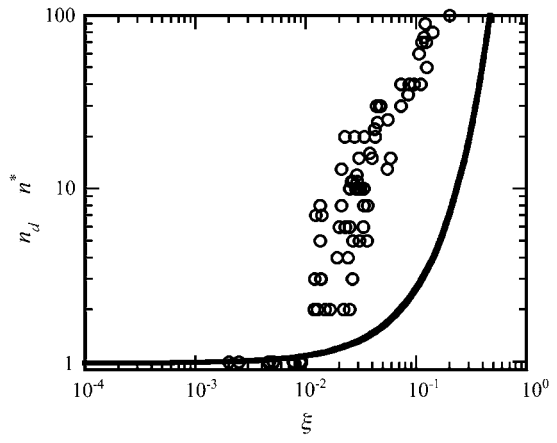

FIGURE 14 Number of trapped domains n_d as a function of excess area ξ. Open circles denote experimentally obtained n_d and solid curve denotes the theoretical prediction based on the free-energy analysis.

$\xi < 0.01$, whereas the vesicles with $\xi > 0.01$ exhibit the trapped coarsening and the number of the trapped domains increases dramatically with increasing ξ. Thus the critical excess area ξ^* is $\sim$0.01.

The transition domain number n_d^* at the transition obtained from our free-energy analysis is plotted against the excess radius ξ by a solid line in Fig. 14. Using the values of $\phi = 0.4$, $\kappa_d/\kappa_m = 1.25$, and $\kappa_d/\sigma = 0.58$ μm, n_d^* is unity up to $\xi \sim 0.01$ and then starts to increase steeply with increasing ξ. This calculation describes the experimental data qualitatively. Thus the domain growth kinetics on a vesicle is governed by the three parameters, κ_d/κ_m, κ_d/σ, and ξ. Here it should be noted that the theoretical critical excess area ξ^* strongly depends on the value of κ_d/σ. Typical values of the bending modulus κ and the line tension σ are $\sim 10^{-19}$ J and $\sim 10^{-11\text{–}12}$ N, respectively. These values give $\kappa_d/\sigma \sim 0.01$–$0.1$ μm, which is an order of magnitude smaller than the used value in this calculation. This deviation may arise from the conventional assumptions used in the model and/or ambiguity in the estimation of κ and σ for the ternary system.

Very recently, a similar slowing down of the domain coarsening was reported for the fluid membranes with asymmetric bilayer using the dissipative particle dynamics simulation(30). In this case, surface tension originated from the spontaneous curvature of the domain brings the long-range repulsive interaction. Thus the coupling of phase separation and elasticity brings anomalous dynamics of the domains on the fluid vesicle.

Experimental conditions for the normal coarsening and the trapped coarsening

Finally we argue about the experimental condition to observe normal coarsening or trapped coarsening. As described before, we observed both coarsening processes in the same microscope field of the same sample. Thus whether it forms the tense vesicle with normal coarsening domains or the flaccid vesicle with trapped coarsening domains seems to depend on the uncontrollable swelling process. Quite recently, however, to form large unilamellar vesicles, a gentle hydration technique using NaI was reported by Tsumoto et al. (31). In this technique, they added NaI methanol solution to the ternary lipid chloroform solution for preparing the dried lipid film, which may control the osmotic pressure difference between the inside and the outside of the vesicle. We found that using this technique, $\sim$90% vesicles show normal coarsening domains, whereas using the standard gentle swelling technique described in the experiment section, $\sim$70% vesicles show trapped coarsening domains. In addition, we examined the excess area of the vesicles produced by the NaI swelling technique and found that most of the vesicles have a small excess radius $\xi < 0.01$. Thus we can control the area/volume ratio of vesicles, and distinguish between normal coarsening and trapped coarsening, by adjusting the ionic strength of NaI solution.

CONCLUSION

We have investigated the growth dynamics of circular domains in the vesicle consisting of DOPC, DPPC, and cholesterol ternary mixture. The coarsening process can be categorized into two types: normal coarsening and trapped coarsening. For normal coarsening, the domains having flat circular shape grow according to the phenomenological power law of $t^{2/3}$. The observed growth law is not described by a two-dimensional diffusion-and-coalescence growth mechanism following the Saffman and Delbrück theory, which may originate from the two-body hydrodynamic interactions between domains. For trapped coarsening, domain coarsening is suppressed by the repulsive interdomain interaction. If the vesicle has enough excess area, the growing domains bud due to the line energy of the domains. The bending of the matrix membrane between the two approaching cap-shaped domains induces the repulsive interdomain interaction. The theoretical calculation based on the budding model reveals that the condition determining whether the vesicle shows trapped coarsening or normal coarsening depends on the excess area of the vesicle, the line tension between phase separating domains, and the bending modulus of the membrane. Thus trapped coarsening is a result of a strong coupling between the phase separation and the elastic nature of the membrane under the area/volume constraint.

We thank Dr. Youhei Fujitani (Keio University) for valuable discussions, and Dr. Norifumi L. Yamada and Mr. Mafumi Hishida for grateful suggestions about NaI.

This work was supported by a Grant-in-Aid for Scientific Research (B) from the Ministry of Education, Science, Sports and Culture of Japan (No. 15340138). A part of this work was carried out when one of the authors (M.Y.) stayed at Yukawa Institute for Theoretical Physics, Kyoto University. She is grateful for the support by the Grant-in-Aid for the 21st Century COE ''Center for Diversity and Universality in Physics'' from the Ministry of Education, Culture, Sports, Science and Technology of Japan.

REFERENCES

1. Simons, K., and E. Ikonen. 1997. Functional rafts in cell membranes. *Nature*. 387:569–572.
2. Brown, D. A., and E. London. 1998. Functions of lipid rafts in biological membranes. *Annu. Rev. Cell Dev. Biol.* 14:111–136.
3. Dietrich, C., L. A. Bagatolli, Z. N. Volovyk, N. L. Thompson, M. Levi, K. Jacobson, and E. Gratton. 2001. Lipid rafts reconstituted in model membranes. *Biophys. J.* 80:1417–1428.
4. Samsonov, A. V., I. Mihalyov, and F. S. Cohen. 2001. Characterization of cholesterol-sphingomyelin domains and their dynamics in bilayer membranes. *Biophys. J.* 81:1486–1500.
5. Kahya, N., D. Scherfeld, K. Bacia, B. Poolman, and P. Schwille. 2003. Probing lipid mobility of raft-exhibiting model membranes by fluorescence correlation spectroscopy. *J. Biol. Chem.* 278:28109–28115.
6. Bagatolli, L. A. 2003. Direct observation of lipid domains in free standing bilayers: from simple to complex lipid mixtures. *Chem. Phys. Lip.* 122:137–145.
7. Veatch, S. L., and S. L. Keller. 2002. Organization in lipid membranes containing cholesterol. *Phys. Rev. Lett.* 89:268101.
8. Veatch, S. L., and S. L. Keller. 2003. Separation of liquid phases in giant vesicles of ternary mixtures of phospholipids and cholesterol. *Biophys. J.* 85:3074–3083.
9. Veatch, S. L., and S. L. Keller. 2005. Seeing spots: complex phase behavior in simple membranes. *Biochim. Biophys. Acta.* 1746: 172–185.
10. Baumgart, T., S. T. Hess, and W. W. Webb. 2003. Imaging coexisting fluid domains in biomembrane models coupling curvature and line tension. *Nature*. 425:821–824.
11. Scherfeld, D., N. Kahya, and P. Schwille. 2003. Lipid dynamics and domain formation in model membranes composed of ternary mixtures of unsaturated and saturated phosphatidylcholines and cholesterol. *Biophys. J.* 85:3758–3768.
12. Lipowsky, R., and R. Dimova. 2003. Domains in membranes and vesicles. *J. Phys. Condens. Matter*. 15:S31–S45.
13. Taniguchi, T. 1996. Shape deformation and phase separation dynamics of two-component vesicles. *Phys. Rev. Lett.* 76:4444–4447.
14. Ayton, G. S., J. L. McWhirter, P. McMurtry, and G. A. Voth. 2005. Coupling field theory with continuum mechanics: a simulation of domain formation in giant unilamellar vesicles. *Biophys. J.* 88:3855–3869.
15. Kumar, P. B. S., G. Gompper, and R. Lipowsky. 2001. Budding dynamics of multicomponent membranes. *Phys. Rev. Lett.* 86:3911–3914.
16. Laradji, M., and P. B. S. Kumar. 2004. Dynamics of domain growth in self-assembled fluid vesicles. *Phys. Rev. Lett.* 93:198105.
17. Laradji, M., and P. B. S. Kumar. 2005. Domain growth, budding, and fission in phase separating self-assembled fluid bilayers. *J. Chem. Phys.* 123:224902.
18. Yamamoto, S., and S. Hyodo. 2003. Budding and fission dynamics of two-component vesicles. *J. Chem. Phys.* 118:7937–7943.
19. Reeves, J. P., and R. M. Dowben. 1969. Formation and properties of thin-walled phospholipid vesicles. *J. Cell. Physiol.* 73:49–60.
20. Needham, D., and E. Evans. 1988. Structure and mechanical properties of giant lipid (DMPC) vesicle bilayers from 20 °C below to 10 °C above the liquid crystal-crystalline phase transition at 24 °C. *Biochemistry*. 27:8261–8269.
21. Henriksen, J. R., and J. H. Ipsen. 2004. Measurement of membrane elasticity by micro-pipette aspiration. *Eur. Phys. J. E.* 14:149–167.
22. Veatch, S. L., and S. L. Keller. 2003. A closer look at the canonical 'raft mixture' in model membrane studies. *Biophys. J.* 84:725–726.
23. Saeki, D., T. Hamada, and K. Yoshikawa. 2006. Domain-growth kinetics in a cell-sized liposome. *J. Phys. Soc. Jap.* 75:013602.
24. Saffman, P. G., and M. Delbrück. 1975. Brownian motion on biological membranes. *Proc. Natl. Acad. Sci. USA*. 72:3111–3113.
25. Komura, S., and K. Seki. 1995. Diffusion constant of a polymer chain in biomembranes. *J. Phys. II. France*. 5:5–9.
26. Furukawa, H. 1985. A dynamic scaling assumption for phase separation. *Adv. Phys.* 34:703–750.
27. Furukawa, H. 1985. Effect of inertia on droplet growth in a fluid. *Phys. Rev. A.* 31:1103–1108.
28. Bastea, S., and J. L. Lebowitz. 1995. Domain growth in computer simulations of segregating two-dimensional binary fluids. *Phys. Rev. E.* 52:3821–3826.
29. Rawicz, W., K. C. Olbrich, T. McIntosh, D. Needham, and E. Evans. 2000. Effect of chain length and unsaturation on elasticity of liquid bilayers. *Biophys. J.* 79:328–339.
30. Laradji, M., and P. B. S. Kumar. 2006. Anomalously slow domain growth in fluid membranes with asymmetric transbilayer lipid distribution. *Phys. Rev. E.* 73:040901.
31. Yamada, N. L., M. Hishida, H. Seto, K. Tsumoto, and T. Yoshikawa. 2006. Unbinding transition induced by osmotic pressure in relation to unilamellar vesicle formation. cond-mat/0607672.